

Dynamics of a charged particle in a magnetic-flux lattice

A. Y. Rom

Department of Chemistry, Technion-Israel Institute of Technology, Haifa 32000, Israel

S. Fishman

Department of Physics, Technion-Israel Institute of Technology, Haifa 32000, Israel

R. Kosloff

Department of Physical Chemistry and the Fritz Haber Research Center, The Hebrew University, Jerusalem 91904, Israel

T. Maniv

Department of Chemistry, Technion-Israel Institute of Technology, Haifa 32000, Israel

(Received 11 January 1996)

The dynamics of a charged particle in a two-dimensional space under the influence of a nonuniform, periodic magnetic field, similar to the magnetic induction inside an extremely type-II superconductor in the vortex state, is studied. The Hamiltonian for this model is found to be classically nonintegrable. A study of classical trajectories shows a global transition from a confined chaotic motion on tori for small amplitude of the periodic modulation, to an extended chaotic system that fills phase space uniformly, for strong modulations. The classical dynamics is confronted with a semiclassical Gaussian wave-packet approach and a time-dependent quantum-mechanical (QM) propagation scheme, for the same Hamiltonian. When the magnetic field modulation is small the envelopes of both the semiclassical and the exact QM autocorrelation functions are found to be Gaussian at short times. For a strong magnetic field modulation the envelope of the semiclassical autocorrelation function crosses over to a decaying exponential, determined by the characteristic Lyapunov exponent of the chaotic motion. It deviates significantly from the exact QM autocorrelation function, which retains the Gaussian envelope. The relatively strong recursion peaks of the latter may indicate a quantum localization effect. [S0163-1829(96)06338-2]

I. INTRODUCTION

In a type-II superconductor below the upper critical field, the magnetic induction is spatially periodic and has the same periodicity as the modulus of the superconducting order parameter.¹ The nonuniform component of the magnetic induction is due to the induced supercurrents generating the vortex lattice. This spatially nonuniform magnetic field can be studied by employing muon-spin rotation (μ^+ SR) techniques as suggested by Brandt.²

The ground state in a periodic magnetic field for a spin- $\frac{1}{2}$ charged particle was obtained analytically by Dubrovin and Novikov.³ Orbital dynamics of spinless charged particles in a random magnetic field was studied recently by Aronov *et al.*,⁴ who showed that in the semiclassical limit the Landau levels, associated with the large uniform component of the magnetic field, undergo a Gaussian broadening in the presence of the nonuniform random component. The problem of a charged particle in a uniform magnetic field with a time-dependent periodic perturbation was studied by Chernikov and co-workers.^{5,6}

In the present paper we focus on the dynamics of a charged particle in a spatially periodic magnetic field similar to that created in the mixed state of type-II superconductors. Using a simple harmonic model for the periodic field component, a detailed study of the classical, semiclassical, and quantum-mechanical dynamics of a spinless charged particle is presented. We have found (1) global transition from con-

finned chaos to extended chaotic behavior in phase space within the framework of classical mechanics; (2) a relation between the Lyapunov exponent and the decay of the semiclassical autocorrelation function envelope; and (3) qualitatively different dynamics of semiclassical Gaussian wave packets and quantum-mechanical wave packets.

The outline of this paper is as follows: Section II treats the classical dynamics properties. Section III presents Heller's-type semiclassical Gaussian wave-packet approach to the problem of a charged particle in the presence of a vector potential. Section IV applies the Chebychev propagation method, discusses the spectral structure, and compares quantum-mechanical and semiclassical results. In Sec. V the Gaussian broadening of Landau levels due to the periodic magnetic field modulation is studied and a summary and discussion conclude this paper.

II. CLASSICAL DYNAMICS OF A CHARGED PARTICLE IN A SPATIALLY PERIODIC MAGNETIC FIELD

The magnetic field model that is studied in the present paper is

$$\mathbf{B} = \left\{ B_0 + B_1 \left(\cos \frac{2\pi x}{a} + \cos \frac{2\pi y}{a} \right) \right\} \hat{z} \quad (1)$$

where B_0 is the uniform component of the magnetic field and B_1 is the amplitude of the magnetic field modulation component. The magnetic field given in Eq. (1) is a simplified

harmonic model for the periodic magnetic field found in a type-II superconductor in the mixed state. Note that in a type-II superconductor the periodic magnetic field has a triangular symmetry rather than a square symmetry, as studied in this paper. This difference in symmetry, however, is not expected to significantly influence the main results of this paper.

The vector potential that generates the above field is given by

$$\mathbf{A} = \left\{ \left(-\frac{1}{2} B_0 y - \frac{a B_1}{2\pi} \sin \frac{2\pi y}{a} \right) \hat{x} + \left(\frac{1}{2} B_0 x + \frac{a B_1}{2\pi} \sin \frac{2\pi x}{a} \right) \hat{y} \right\} \quad (2)$$

and the classical Hamiltonian is

$$H(\mathbf{p}, \mathbf{r}) = \frac{1}{2m} \left(\mathbf{p} - \frac{q}{c} \mathbf{A} \right)^2, \quad (3)$$

where q is the electric charge of the particle, and m its mass.

The Lorentz equation for a charged particle in the magnetic field given in Eq. (1) is

$$\dot{v}_x = \omega_c v_y + \omega_1 \left(\cos \frac{2\pi x}{a} + \cos \frac{2\pi y}{a} \right) v_y, \quad (4a)$$

$$\dot{v}_y = -\omega_c v_x - \omega_1 \left(\cos \frac{2\pi x}{a} + \cos \frac{2\pi y}{a} \right) v_x, \quad (4b)$$

where $\omega_c = qB_0/mc$ and $\omega_1 = qB_1/mc$.

The Hamiltonian [Eq. (3)] with $B_1=0$ corresponds to a charged particle in a uniform magnetic field. The energy, $E_0 = H(\mathbf{p}, \mathbf{r})$, and the angular momentum, $L_z = xP_y - yP_x$, are its two constants of motion. In this case the Hamiltonian is integrable and degenerate since the cyclotron frequency is independent of x, y, P_x, P_y . This degeneracy implies a high sensitivity to perturbations as described by Zaslavski and co-workers.^{5,6}

It should be stressed here that the size a of the unit cell in the Abrikosov lattice depends on the intensity of the external magnetic field, represented in our model by B_0 . Specifically, a unit cell in the corresponding flux lattice is threaded by a single Cooper-pair flux quantum, $\phi_0 = hc/2e$, which means that $a = \sqrt{hc/2eB_0}$. On the other hand, the charge q of the particle determines another length, that is, the magnetic length $l_{B_0} = \sqrt{c\hbar/qB_0}$. The ratio $q/2e = a^2/2\pi l_{B_0}^2$, which is equal to the magnetic flux through a unit cell per flux quantum of the particle, is an important parameter determining the energy spectrum of the particle.

The motion in phase space of a two-dimensional (2D) integrable Hamiltonian system is on a 2D torus where the Poincaré surface of section is a slice of this torus. The initial position in phase space defines a torus on which the classical orbit lies. For a nonintegrable Hamiltonian system the existence of tori which confine the phase space flow is not guaranteed. Kolmogorov-Arnold-Moser (KAM) theory, when applicable, states that most of the tori are preserved for a sufficiently weak perturbation on the integrable Hamiltonian. The KAM theory does not apply to the Hamiltonian of a charged particle in a uniform magnetic field with an addi-

tional perturbation, since the nondegeneracy condition required by the theory is violated.⁵

In the presence of the magnetic field [Eqs. (2) and (3)] the Hamiltonian is not integrable, but for small values of B_1 the phase space motion is almost entirely on tori. Figure 1(a) shows the surface of a section of 100 trajectories with the same energy but different initial positions in phase space. For larger values of B_1 , a few tori are destroyed and the surface of section shows the preserved tori and phase space areas with disordered points which are characteristic of a chaotic motion [see Figs. 1(b) and 1(c)]. For even larger values of B_1 , almost all the tori are destroyed. The motion is chaotic almost in all phase space.

The Poincaré surface of section [Figs. 1(a)–1(c)] shows a global transition from confined to extended chaos as a function of the flux lattice amplitude B_1 . This transition is studied below by the calculation of the Lyapunov exponent, averaged over phase space.

An important characteristic of a chaotic motion is the great sensitivity of the motion to small changes in the initial conditions. Closely neighboring trajectories are found to diverge exponentially in chaotic systems. The Lyapunov exponent measures the mean rate of exponential separation of neighboring trajectories. For regular motion the exponent is zero since the trajectories separate only linearly in time (see, for example, Ref. 7). The Lyapunov exponents are calculated by a linearization of the equations of motion around the classical trajectory.

A normalized deviation from the classical trajectory vector in phase space is defined:

$$\delta \mathbf{t} = N \{ \delta x \hat{x} + \delta y \hat{y} + \delta p_x \hat{p}_x + \delta p_y \hat{p}_y \}. \quad (5)$$

Its equations of motion are derived by linearization of the equations of motion in the four-dimensional phase space and are given in terms of the Hamiltonian second derivatives:

$$\frac{\partial}{\partial t} \begin{pmatrix} \delta x \\ \delta y \\ \delta p_x \\ \delta p_y \end{pmatrix} = \begin{pmatrix} \frac{\partial^2 H}{\partial p_x \partial x} & \frac{\partial^2 H}{\partial p_x \partial y} & \frac{\partial^2 H}{\partial p_x^2} & \frac{\partial^2 H}{\partial p_x \partial p_y} \\ \frac{\partial^2 H}{\partial p_y \partial x} & \frac{\partial^2 H}{\partial p_y \partial y} & \frac{\partial^2 H}{\partial p_y^2} & \frac{\partial^2 H}{\partial p_y \partial p_x} \\ -\frac{\partial^2 H}{\partial x^2} & -\frac{\partial^2 H}{\partial x \partial y} & -\frac{\partial^2 H}{\partial x \partial p_x} & -\frac{\partial^2 H}{\partial x \partial p_y} \\ -\frac{\partial^2 H}{\partial y \partial x} & -\frac{\partial^2 H}{\partial y^2} & -\frac{\partial^2 H}{\partial y \partial p_x} & -\frac{\partial^2 H}{\partial y \partial p_y} \end{pmatrix} \times \begin{pmatrix} \delta x \\ \delta y \\ \delta p_x \\ \delta p_y \end{pmatrix}. \quad (6)$$

The largest Lyapunov exponent is calculated from the definition:

$$\lambda = \lim_{t \rightarrow \infty} \frac{\ln |\delta \mathbf{t}(t)|}{t}. \quad (7)$$

With the magnetic flux lattice model Hamiltonian [Eq. (3)], the nonvanishing terms in Eq. (6) are

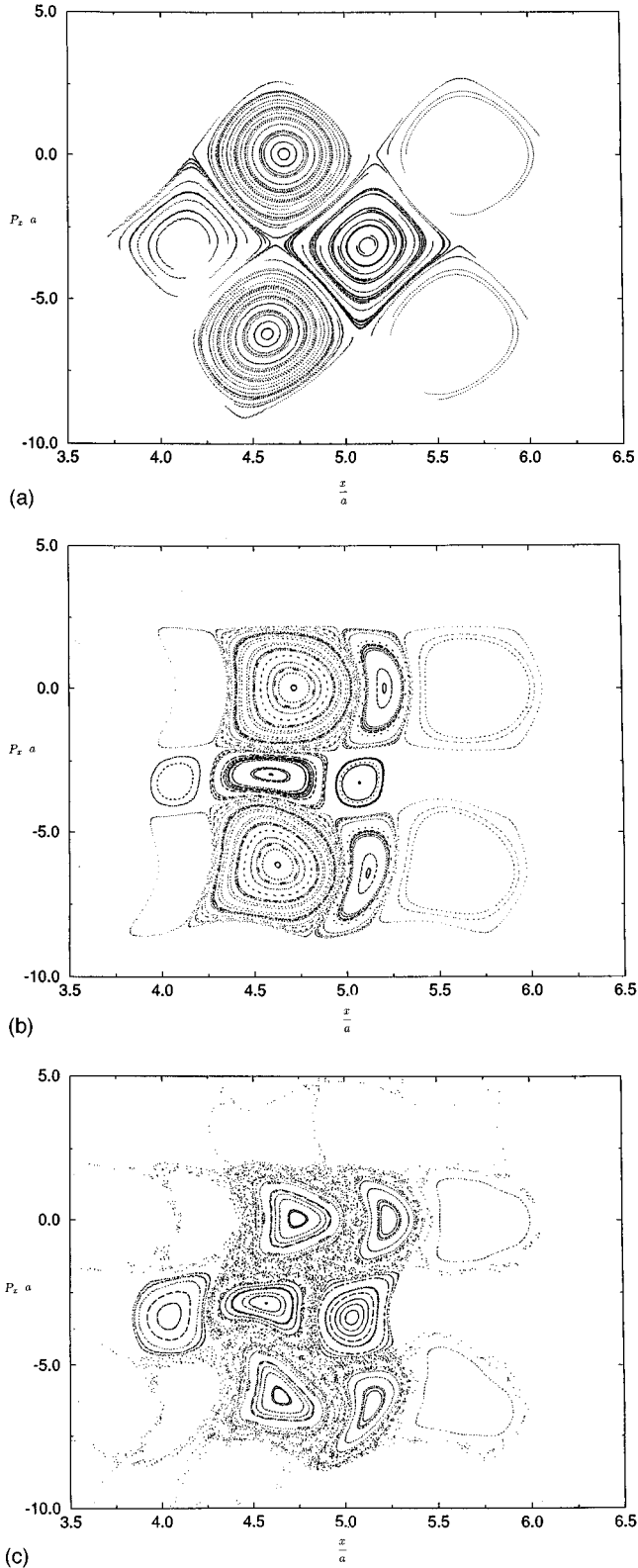


FIG. 1. Poincaré surface of section of 100 equienergy trajectories launched from different positions in a magnetic unit cell. (a) $B_1/B_0=0.01$, (b) $B_1/B_0=0.05$, and (c) $B_1/B_0=0.08$. For (a)–(c) $E_0=100\hbar\omega_c$. In (a) motion on tori is seen. The separating lines can also be observed as the separating lines between different clusters of tori centered around adjacent fixed points in the phase space. In (b) and (c) filled areas in phase space between the remaining tori are seen indicating the existence of chaotic motion.

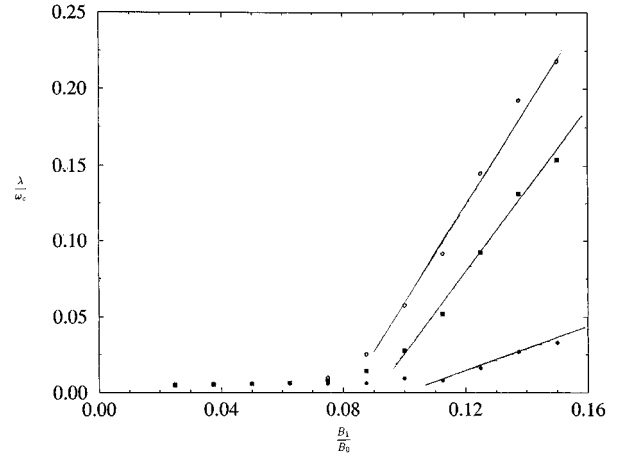


FIG. 2. Lyapunov exponent averaged over phase space for three values of the energy: 25, 50, and 100 in units of $\hbar\omega_c$. For each curve the transition from a confined chaotic motion to extended chaotic motion is seen as a linear rise in the averaged Lyapunov exponent for large enough values of B_1 . With a larger value of the energy the transition occurs at smaller values of B_1 .

$$\frac{\partial^2 H}{\partial p_x \partial y} = \frac{1}{m} \frac{q}{c} \left(\frac{1}{2} B_0 + B_1 \cos \frac{2\pi y}{a} \right), \quad (8a)$$

$$\frac{\partial^2 H}{\partial p_x^2} = \frac{1}{m}, \quad (8b)$$

$$\frac{\partial^2 H}{\partial p_y \partial x} = -\frac{1}{m} \frac{q}{c} \left(\frac{1}{2} B_0 + B_1 \cos \frac{2\pi x}{a} \right), \quad (8c)$$

$$\frac{\partial^2 H}{\partial p_y^2} = \frac{1}{m}, \quad (8d)$$

$$\begin{aligned} -\frac{\partial^2 H}{\partial x^2} = & -\frac{1}{2m} \frac{q^2}{c} \left(\frac{1}{2} B_0^2 + 2B_1^2 \cos \frac{4\pi x}{a} + 2B_0 B_1 \cos \frac{2\pi x}{a} \right) \\ & - \frac{q}{c} B_1 \frac{2\pi}{a} \frac{1}{m} \left(p_y - \frac{1}{2} \frac{q}{c} B_0 x \right) \sin \frac{2\pi x}{a}, \end{aligned} \quad (8e)$$

$$\begin{aligned} -\frac{\partial^2 H}{\partial y^2} = & -\frac{1}{2m} \frac{q^2}{c} \left(\frac{1}{2} B_0^2 + 2B_1^2 \cos \frac{4\pi y}{a} + 2B_0 B_1 \cos \frac{2\pi y}{a} \right) \\ & + \frac{q}{c} B_1 \frac{2\pi}{a} \frac{1}{m} \left(p_x + \frac{1}{2} \frac{q}{c} B_0 y \right) \sin \frac{2\pi y}{a}. \end{aligned} \quad (8f)$$

The Lyapunov exponent vanishes when the motion is on tori and is positive for a chaotic trajectory. Since it was shown by the Poincaré surface of section [Figs. 1(a)–1(c)] that as B_1 is increased some tori are preserved and others are destroyed, an average over phase space has to be calculated in order to determine the global transition from a regular motion (on tori) to an extended chaotic motion in phase space.

In Fig. 2 an average Lyapunov exponent, over the same 100 trajectories that were presented in the Poincaré surface of section, are shown with three energies 25, 50, and 100 in units of $\hbar\omega_c$. For small values of B_1 the calculation of the Lyapunov exponent [Eqs. (5)–(7)] does not converge to a

constant value for long propagation times. Since it decreases to zero very slowly we did not determine whether the Lyapunov exponent vanishes exactly or it is very small. For large values of B_1 the calculation does converge to a constant value which is the largest Lyapunov exponent. The transition to extended chaotic motion is seen as an approximate linear rise in the average value of λ as a function of the lattice parameter B_1 above some critical value of B_1 . The critical field is determined by linearly extrapolating the Lyapunov exponent values at high values of B_1 to zero. The critical field of the transition exhibits an inverse dependence on energy. At small energies the transition occurs at higher values of B_1 .

With the magnetic flux lattice classical Hamiltonian [Eqs. (2) and (3)], each classical trajectory has an infinite number of equivalent trajectories that are obtained by magnetic translations. The magnetic translation shifts the initial space coordinate by a unit cell vector and conserves the initial velocity components by an appropriate shift of the initial generalized momentum components. The magnetic translations are

$$x'_0 = x_0 + ja, \quad (9a)$$

$$y'_0 = y_0 + la, \quad (9b)$$

$$p'_{x0} = p_{x0} - l \frac{1}{2} B_0 \frac{q}{c} a, \quad (9c)$$

$$p'_{y0} = p_{y0} + j \frac{1}{2} B_0 \frac{q}{c} a. \quad (9d)$$

The magnetic translation symmetry and the existence of equivalent trajectories are the reason for the periodicity seen in the Poincaré surface of section [see Fig. 1(a)]. The classical magnetic translation symmetry of the magnetic-flux lattice model exhibits itself also in the calculation of Lyapunov exponents and in the semiclassical Gaussian time-dependent wave-packet approach. In both cases the equations of motion are invariant under the magnetic translations, and hence equivalent trajectories have an identical stability character, determined by the Lyapunov exponent, and an identical time-dependent Gaussian wave packet (up to a phase) that follows the classical trajectory.

From the quantum-mechanical point of view the presence of magnetic translational symmetry means that tunneling between equivalent closed orbits should lead to the broadening of the Landau levels, associated with the ideal cyclotron orbits of the particle in the uniform magnetic field B_0 , into energy bands. Dubrovin and Novikov³ showed that each Landau band splits into m magnetic subbands in the presence of a periodic magnetic field modulation, where m is the number of magnetic flux quanta that threads through a unit cell (m is an integer larger than 1). In this paper the focus is not on the internal fine structure of the energy bands, thus for the sake of simplicity the unit cell length is $a = \sqrt{\hbar c / e B_0}$, providing one magnetic flux quanta per unit cell and a simply broadened Landau bands.

The Poincaré surface of section for a two degrees of freedom integrable bound Hamiltonian system produces clusters of tori centered around different stable fixed points on which

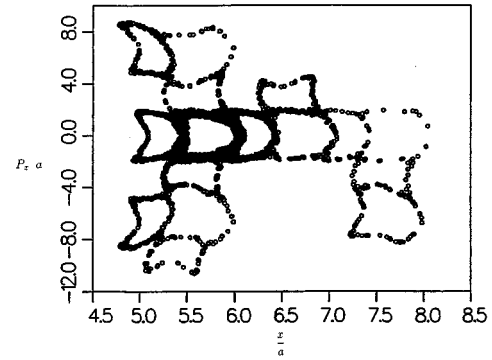


FIG. 3. Zaslavski's web explored by a single trajectory. At each hole of the web there is a fixed point and the web structure is a separatrix sheet between the fixed points. $E = 100\hbar\omega_c$ and $B_1/B_0 = 0.08$.

the trajectories lie, and are separated by sharp separatrix lines. If a perturbation is added to the Hamiltonian, chaotic trajectories appear in the vicinity of the separatrix lines of the unperturbed Hamiltonian. A single trajectory initialized in the vicinity of the separatrix line can explore phase space by moving in the regime in phase space that is created by the destruction of the separatrix line. This phenomenon was found by Zaslavski^{5,6} in a system of a charged particle in a uniform magnetic field with a time-dependent periodic perturbation, and is referred to as Zaslavski's web. The formation of the web changes the transport properties of the system since these specific trajectories are classically unbound, while the trajectories in the unperturbed system (a uniform magnetic field) are classically bound. When B_1 is small, the regime of the destroyed separatrix is exponentially small in phase space, nearly all the trajectories seen in Fig. 1(a) lie on tori and the web is not observed. With larger B_1 values there are regimes in phase space that are filled [in the Poincaré surface of section, Figs. 1(b)–1(c)] and in these regimes a single trajectory can explore phase space and by that explore the web structure. In Fig. 3 Zaslavski's web is shown to be created by a single trajectory. In each hole of the web there is a fixed point and the web is a separatrix sheet between the fixed points. (The fixed point can be observed as the center of many localized trajectories that encircle the fixed point. These trajectories are not shown in Fig. 3.)

III. SEMICLASSICAL GAUSSIAN TIME-DEPENDENT WAVE-PACKET APPROACH

The classical dynamics is confronted with a semiclassical propagation on the same Hamiltonian describing a charged particle in the presence of a vector potential. Heller's-type semiclassical time-dependent Gaussian wave-packet approach is employed.⁸

$$\psi(\mathbf{r}, t) = \exp\left\{ \frac{i}{\hbar} \gamma_t + \frac{i}{\hbar} \mathbf{p}_t(\mathbf{r} - \mathbf{r}_t) + \frac{i}{\hbar} (\mathbf{r} - \mathbf{r}_t) \alpha_t(\mathbf{r} - \mathbf{r}_t) \right\}, \quad (10)$$

where $\gamma_t, \mathbf{r}_t, \mathbf{p}_t, \alpha_t$ are all time-dependent parameters determined by first-order differential equations that are derived below. The vector potential $\mathbf{A}=(A_x, A_y, 0)$ is expanded in Taylor series around the instantaneous center of the wave packet, \mathbf{r}_t , which follows the classical trajectory

$$\begin{aligned} A_x(x, y) &= A_x|_{\mathbf{r}_t} + \frac{\partial A_x}{\partial x} \Big|_{\mathbf{r}_t} (x - x_t) + \frac{\partial A_x}{\partial y} \Big|_{\mathbf{r}_t} (y - y_t) \\ &+ \frac{1}{2} \frac{\partial^2 A_x}{\partial x^2} \Big|_{\mathbf{r}_t} (x - x_t)^2 + \frac{1}{2} \frac{\partial^2 A_x}{\partial y^2} \Big|_{\mathbf{r}_t} (y - y_t)^2 \\ &+ \frac{\partial^2 A_x}{\partial x \partial y} \Big|_{\mathbf{r}_t} (x - x_t)(y - y_t), \end{aligned} \quad (11a)$$

$$\begin{aligned} A_y(x, y) &= A_y|_{\mathbf{r}_t} + \frac{\partial A_y}{\partial x} \Big|_{\mathbf{r}_t} (x - x_t) + \frac{\partial A_y}{\partial y} \Big|_{\mathbf{r}_t} (y - y_t) \\ &+ \frac{1}{2} \frac{\partial^2 A_y}{\partial x^2} \Big|_{\mathbf{r}_t} (x - x_t)^2 + \frac{1}{2} \frac{\partial^2 A_y}{\partial y^2} \Big|_{\mathbf{r}_t} (y - y_t)^2 \\ &+ \frac{\partial^2 A_y}{\partial x \partial y} \Big|_{\mathbf{r}_t} (x - x_t)(y - y_t), \end{aligned} \quad (11b)$$

The Gaussian wave packet is substituted into the time-dependent Schrödinger equation

$$i\hbar \frac{\partial \psi(\mathbf{r}, t)}{\partial t} = \frac{1}{2m} \left(-i\hbar \nabla - \frac{q}{c} \mathbf{A} \right)^2 \psi(\mathbf{r}, t). \quad (12)$$

First-order equations of motion are derived for the time-dependent functions of the Gaussian wave packet by equating terms of the same order in the deviation from the classical trajectory [all terms proportional to $(x - x_t)$, $(y - y_t)$, $(x - x_t)^2$, $(y - y_t)^2$, $(x - x_t)(y - y_t)$, and the free terms]. The set of differential equations for the Gaussian time-dependent functions are

$$\dot{\gamma}_t = \mathbf{p}_t \cdot \dot{\mathbf{r}}_t - E + \frac{i\hbar}{m} (\alpha_{11} + \alpha_{22}), \quad (13a)$$

$$m\ddot{\mathbf{r}}_t = \frac{q}{c} \dot{\mathbf{r}}_t \times \mathbf{B}, \quad (13b)$$

$$\begin{aligned} \dot{\alpha}_{11} &= -\frac{2}{m} \left(\alpha_{11} - \frac{1}{2} \frac{q}{c} \frac{\partial A_x}{\partial x} \right)^2 - \frac{1}{2m} \left(\alpha_{12} - \frac{q}{c} \frac{\partial A_y}{\partial x} \right)^2 \\ &+ \frac{1}{2} \frac{q}{c} \left(\dot{x}_t \frac{\partial^2 A_x}{\partial x^2} + \dot{y}_t \frac{\partial^2 A_y}{\partial x^2} \right), \end{aligned} \quad (13c)$$

$$\begin{aligned} \dot{\alpha}_{22} &= -\frac{2}{m} \left(\alpha_{22} - \frac{1}{2} \frac{q}{c} \frac{\partial A_y}{\partial y} \right)^2 - \frac{1}{2m} \left(\alpha_{12} - \frac{q}{c} \frac{\partial A_x}{\partial y} \right)^2 \\ &+ \frac{1}{2} \frac{q}{c} \left(\dot{x}_t \frac{\partial^2 A_x}{\partial y^2} + \dot{y}_t \frac{\partial^2 A_y}{\partial y^2} \right), \end{aligned} \quad (13d)$$

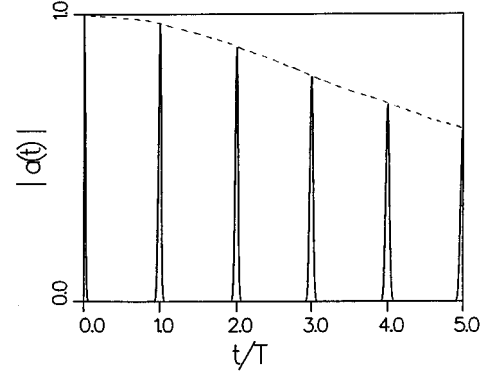


FIG. 4. The semiclassical autocorrelation function showing a Gaussian envelope of the recursions peaks, $E=100\hbar\omega_c$ and $B_1/B_0=0.025$.

$$\begin{aligned} \dot{\alpha}_{12} &= -\frac{2}{m} \left(\alpha_{11} - \frac{1}{2} \frac{q}{c} \frac{\partial A_x}{\partial x} \right) \left(\alpha_{12} - \frac{q}{c} \frac{\partial A_x}{\partial y} \right) \\ &- \frac{2}{m} \left(\alpha_{22} - \frac{1}{2} \frac{q}{c} \frac{\partial A_y}{\partial y} \right) \left(\alpha_{12} - \frac{q}{c} \frac{\partial A_y}{\partial x} \right) \\ &+ \frac{q}{c} \left(\dot{x}_t \frac{\partial^2 A_x}{\partial x \partial y} + \dot{y}_t \frac{\partial^2 A_y}{\partial x \partial y} \right), \end{aligned} \quad (13e)$$

with the definitions

$$m\dot{\mathbf{r}}_t = \mathbf{p}_t - \frac{q}{c} \mathbf{A}_t, \quad (13f)$$

$$E = \frac{1}{2} m \dot{\mathbf{r}}_t^2. \quad (13g)$$

The main feature of this semiclassical approximate wave packet is that it remains of Gaussian shape at all times. During propagation its spatial width varies, its momentum vector can change direction and magnitude, and the total phase changes, but it remains a Gaussian shaped centered at the classical trajectory spatial position. The Gaussian form allows analytical calculation of spatial integrals over the wave packet which are needed for calculating the autocorrelation function. The disadvantage of the Gaussian wave-packet approach is that no bifurcation of the wave packet is allowed. This can cause significant deviations from the exact quantum-mechanical wave-packet dynamics.

The overlap between the initial wave packet and the propagated one at any time t is the autocorrelation function

$$a(t) = \langle \psi(r, 0) | \psi(r, t) \rangle. \quad (14)$$

Using the Gaussian form of the wave packet, given by Eq. (10), the spatial overlap integral is calculated analytically. The absolute values of the autocorrelation function are shown in Figs. 4 and 5, for the first five periods with two values of B_1 . For small values of B_1 the envelope of the recursions peaks at short propagation times has a Gaussian shape (see Fig. 4). For larger values of B_1 , the envelope has an exponential decay form shown as the dotted line in Fig. 5, taking the form,

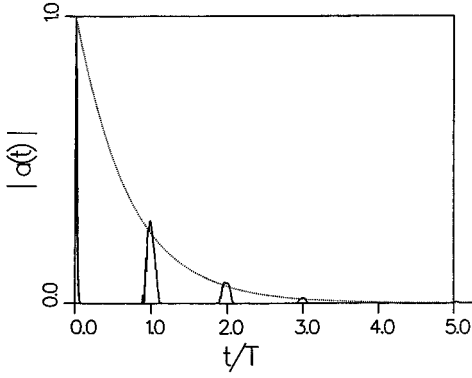


FIG. 5. The semiclassical autocorrelation function (solid line) and an exponential envelope with the calculated Lyapunov exponent $\lambda/\omega_c=0.223$ (dotted line). $E=100\hbar\omega_c$ and $B_1/B_0=0.15$.

$$A = e^{-\lambda t}. \quad (15)$$

The value of λ is the average Lyapunov exponent calculated at the same value of B_1 . The correspondence between the exponential decay of the autocorrelation function with the average Lyapunov exponent is good (see Fig. 5). Our conclusion from this correspondence is that in the chaotic regime the Lyapunov exponent determines the decay of the semiclassical autocorrelation function. In Sec. IV it will be shown that the quantum-mechanical autocorrelation function does not decay exponentially in the classically chaotic regime. Thus, the quantum-mechanical and the semiclassical autocorrelation functions are qualitatively different.

IV. CONVERGED QUANTUM-MECHANICAL WAVE-PACKET DYNAMICS ON A GRID BY THE CHEBYCHEV PROPAGATION METHOD

The Chebychev propagation scheme¹²⁻¹⁴ provides a uniformly convergent scheme for the time-dependent Schrödinger equation allowing us to obtain accuracy limited only by the computers precision. This approach and other related methods are widely used to perform numerically converged quantum-mechanical calculations in various areas of quantum molecular dynamics. A brief presentation of the method is given below. The Schrödinger equation has the following formal solution for a time-independent Hamiltonian:

$$\psi(\mathbf{r}, t) = \hat{U}(t) \psi(\mathbf{r}, 0), \quad (16)$$

where $\hat{U}(t)$ is the evolution operator

$$\hat{U}(t) = \exp\left(-i\hat{H}\frac{t}{\hbar}\right). \quad (17)$$

The Chebychev propagation scheme is based on a converged polynomial expansion of the evolution operator. The wave packet at time t is given by

$$\psi(\mathbf{r}, t) = \exp(-i\alpha) \sum_n a_n(\alpha) \phi_n, \quad (18a)$$

where $\alpha = \Delta E t / 2\hbar$,

$$a_n(\alpha) = \begin{cases} 2J_n(\alpha) & \text{if } n > 0, \\ J_0(\alpha) & \text{if } n = 0. \end{cases} \quad (18b)$$

$J_n(\alpha)$ is the first kind of Bessel function of an integer order. The matrix ϕ_n is calculated by the Chebychev recursion formula

$$\phi_{n+1} = 2i\hat{H}_{\text{norm}}\phi_n - \phi_{n-1}. \quad (19)$$

\hat{H}_{norm} is a shifted and normalized Hamiltonian operator such that its eigenvalues are spread within the interval $[-1, 1]$, where the Chebychev polynomials are defined. Convergence of the sum in Eq. (18a) is reached when n , the order of the Chebychev polynomial, is greater than α . This is due to the fact that Bessel functions decay exponentially when their order is greater than its argument. The basic operation of the Hamiltonian on the wave packet at the grid points is a sum of local potential energy operators, and nonlocal kinetic-energy operators which are calculated in the momentum space by a fast Fourier transform algorithm following Kosloff and Kosloff.¹¹

The spectrum of the Hamiltonian is calculated from the autocorrelation function as follows: During propagation operation an overlap vector P is calculated. The autocorrelation function is given in terms of the overlap vector components by

$$P_n = \langle \phi_0 | \phi_n \rangle, \quad (20a)$$

$$a(t) = \langle \psi(r, 0) | \psi(r, t) \rangle = \exp(-i\alpha) \sum_n a_n(\alpha) P_n. \quad (20b)$$

The calculation of the Fourier transform of the autocorrelation function reduces in this scheme to a Fourier transform of the Bessel function that is given below.^{13,14}

$$a(\omega) = \int_0^\infty a(t) e^{i\omega t} dt = \sum_n c_n(\beta) P_n, \quad (21a)$$

where

$$c_0(\beta) = \frac{2}{\sqrt{1-\beta^2}}, \quad (21b)$$

$$\beta = \frac{2\hbar(\omega - \omega_0)}{\Delta E}, \quad (21c)$$

$$\omega_0 = \frac{\Delta E}{2\hbar}, \quad (21d)$$

$$c_n(\beta) = \begin{cases} \frac{4 \cos[n \sin^{-1}(\beta)]}{\sqrt{1-\beta^2}} & \text{if } n \text{ is even,} \\ \frac{4 \sin[n \sin^{-1}(\beta)]}{\sqrt{1-\beta^2}} & \text{if } n \text{ is odd.} \end{cases} \quad (21e)$$

High-resolution spectra using the Chebychev propagation scheme are presented in Ref. 15, where the ground state in a periodic magnetic field is studied.

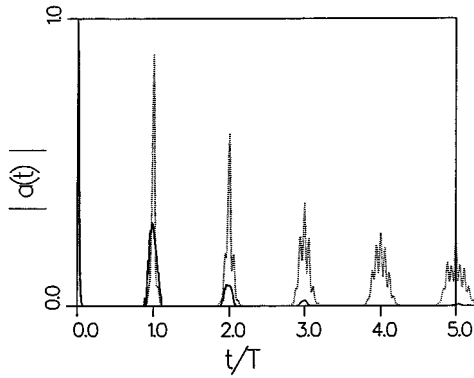


FIG. 6. The semiclassical autocorrelation function (solid line) vs the quantum one (dotted line). The semiclassical autocorrelation function has an exponential envelope while the quantum one has much stronger recursion peaks and it retains its Gaussian envelope.

Comparing the converged quantum autocorrelation function with the semiclassical one for a small flux lattice amplitude, B_1 , the quantum autocorrelation function has at each time period a stronger recursion peak. Both autocorrelation functions show a Gaussian envelope determined by the values of the recursions peaks. When a larger amplitude of the flux is used ($B_2/B_0=0.15$ in Fig. 6), the envelope of the semiclassical autocorrelation function becomes an exponentially decaying function, determined by the Lyapunov exponent, while the quantum-mechanical autocorrelation function retains the Gaussian envelope structure obtained with small values of B_1 .

The Gaussian wave packet follows the chaotic classical trajectory and the Gaussian width differential equations are closely related to the stability differential equation of a trajectory that is solved in the calculation of the Lyapunov exponent [Eq. (6)]. Heller in his review¹⁰ shows the relations between the Gaussian wave packet and the elements of the monodromy matrix, which is related to the stability of the classical trajectory measured by the Lyapunov exponent. This relation might be the reason for the general good agreement between the autocorrelation envelope exponential decay with the Lyapunov exponent calculation. Thus the semiclassical Gaussian wave packet reflects the classical dynamics of the system.

The exact quantum-mechanical wave packet does not follow the route of a single classical trajectory. It can bifurcate and interfere with making the dynamics persistent to the classical chaotic behavior of the system. The strong recursion peaks obtained by the exact autocorrelation function in comparison to the semiclassical one are due to interferences that are taken fully into account by the converged Chebychev propagation and are not described well by the approximated Gaussian wave packet. This result might indicate a quantum localization of the charged particle in the studied magnetic flux lattice model, which elucidation needs a more detailed investigation.

In Fig. 7 the absolute value of the autocorrelation function is shown. There are three time scales that characterize the behavior of the autocorrelation function (see Heller⁹). The

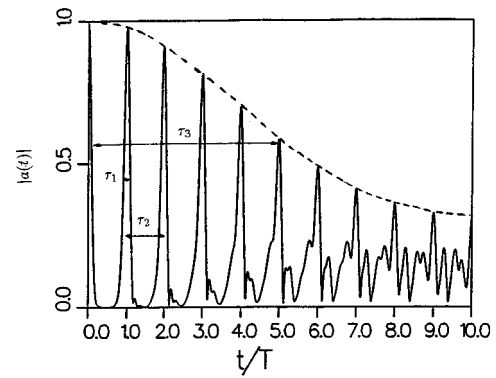


FIG. 7. The modulus of the autocorrelation function in the first ten periods. The three time scales τ_1 , τ_2 , and τ_3 are seen. $E=100\hbar\omega_c$ and $B_1/B_0=0.15$.

shortest time scale, τ_1 , determined by the half width at half maximum of a single recursion peak, is related to the broadest feature in the energy domain, which is the energy width of the initial wave packet. The second time scale, τ_2 , is the time separation between the recursions peaks, and is related to the energy level spacing of $\hbar\omega_c$, where $\omega_c=2\pi/\tau_2$ is the cyclotron frequency. The third time scale, τ_3 , is determined by the Gaussian envelope created by the maxima of the recursions peaks every time period τ_2 . The time scale τ_3 is related to the broadening of Landau levels due to B_1 .

In a plot of $-\ln(|a(t)|)$ vs t^2 , the recursion peaks of the autocorrelation function seen in Fig. 7 appear as a set of minima. If the autocorrelation function has a Gaussian envelope at short propagation time, the minima of the logarithm plot will fit a straight line whose slope is $1/\tau_3^2$. In Fig. 8 the minima are linear in t^2 and the relaxation time can be extracted. For long propagation times the envelope of the autocorrelation function does not have a simple Gaussian form. The exact structure of the autocorrelation function for long times is related to the fine structure of the Hamiltonian spectrum. A high resolution spectrum can be obtained by a Fourier transform of the autocorrelation function with long time propagation.

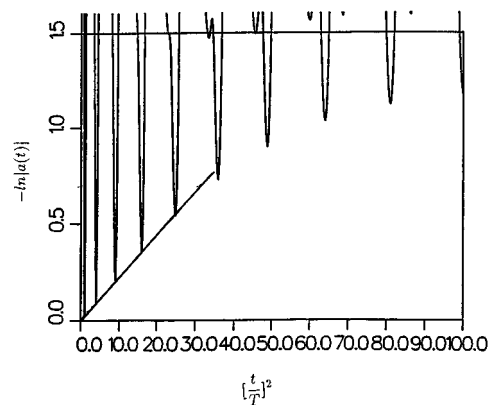


FIG. 8. The logarithmic plot of the modulus of the autocorrelation function vs t^2 showing the Gaussian behavior at short times. The scattering rate $1/\tau_3^2$ is determined from the slope. $E=100\hbar\omega_c$ and $B_1/B_0=0.15$.

V. LANDAU LEVEL GAUSSIAN BROADENING

An overview of magnetic oscillations in metals is given by Shonberg (see Ref. 16). An important example of magnetic oscillations is the de Haas–van Alphen effect which is used to study Fermi surfaces in metals and, recently, type-II superconductors.^{17–22} The effect of Landau level broadening, due to finite temperature, impurities, and inhomogeneous magnetic field, on the magnetization of a two-dimensional electron gas was studied by Shonberg.²³ In this paper Landau level broadening due to an additional periodic component of the magnetic field is studied by examining the characteristics of an autocorrelation function [see Eq. (14)] in the time domain.

The third time scale, τ_3 , that was defined in the previous section and which is related to the broadening of Landau levels, is determined by the Gaussian envelope of the autocorrelation function at short propagation times

$$A_{\text{envelope}} = \exp\left(\frac{-t^2}{\tau_3^2}\right). \quad (22)$$

The width of the broadened Landau levels is given by

$$\frac{\Delta\omega}{\omega_c} = \frac{\pi}{\tau_3\omega_c}. \quad (23)$$

Fitting our numerical result for the envelope of the autocorrelation function to the Gaussian (22) with various values of B_1 and E_0 (see, for example, Figs. 7 and 8), we find the following analytical expression for the Landau levels width:

$$\frac{\pi}{\tau_3\omega_c} = 0.351 \left(\frac{E_0}{\hbar\omega_c}\right)^{1/4} \frac{B_1}{B_0}, \quad (24)$$

where E_0 is the mean energy of the initial Gaussian wave packet.

It is instructive to compare this result to the expression for the Landau level width derived by Aronov *et al.*,⁴ in a model similar to that used here, but with a completely random distribution of flux lines. These authors have found that in the semiclassical limit, the mean local density of states (obtained by averaging over the realizations of the flux lines configurations) has a Gaussian line shape, with a Landau level width given by

$$\frac{\pi}{\tau\omega_c} = \left(\frac{mE_0}{\hbar^2}\right)^{1/2} \frac{\sqrt{\langle b^2 \rangle}}{B_0}, \quad (25)$$

where $\langle b^2 \rangle = \int \langle B_1(\mathbf{r})B_1(\mathbf{r}') \rangle d^2r'$, which is proportional to the mean-square amplitude of the random field fluctuations.

The amplitude B_1 of the periodic modulation in our model may be related to $\langle b^2 \rangle$ in the random flux lines model by $\langle b^2 \rangle = B_1^2 l_{B_0}^2$, where $l_{B_0} = \sqrt{c\hbar/eB_0} = a/\sqrt{2\pi}$ is the magnetic length. Thus the corresponding linewidth [Eq. (25)] may be written as

$$\frac{\pi}{\tau\omega_c} = \left(\frac{E_0}{\hbar\omega_c}\right)^{1/2} \frac{B_1}{B_0}. \quad (26)$$

In the semiclassical limit, considered in both models, the ratio $E_0/\hbar\omega_c$ is much larger than unity. Thus the inhomogeneous broadening of the Landau levels by a random distribution of flux lines is much stronger than the broadening by a regular flux lattice.

VI. SUMMARY AND DISCUSSION

We have shown that the classical Hamiltonian of a charged particle in the presence of a small, spatially periodic magnetic field, superimposed on a large uniform magnetic field, is chaotic. A detailed analysis of the Poincaré surfaces for the classical dynamics and the corresponding Lyapunov exponents has been made. An extended web in the Poincaré map, similar to that found by Zaslavski for a charged particle in a uniform magnetic field, with a time-dependent periodic perturbation, is found in the stationary, spatially periodic magnetic field model studied here. The formation of the web is expected to change the transport properties of the system since the specific trajectories involved are classically unbound, while the trajectories in the unperturbed system (a uniform magnetic field), and also most of the trajectories with a small perturbation, are classically bound. It is not clear, however, to what extent this remarkable effect can survive the influence of the full quantum-mechanical bifurcation and interference of the wave packet, neglected in the classical description.

We have found that the envelope of the semiclassical autocorrelation function obtained by the semiclassical Gaussian wave-packet approach is determined by Lyapunov exponent in the chaotic regime. The exact quantum-mechanical autocorrelation function envelope does not decay exponentially and it has much stronger recursion peaks than the semiclassical one. The dynamics of wave packets was used to estimate the spectrum that is obtained with limited resolution. A qualitative difference between the quantum and semiclassical linewidths was found. The semiclassical result may be relevant if weak noise, leading to decoherence is present. We have shown that as for a random flux line distribution, the inhomogeneous broadening of the Landau levels by a periodic magnetic field component is Gaussian, but with a much smaller linewidth.

Experimental testing of the model studied here seems to be feasible for charged particles like muons (μ^+). These charged, massive particles ($m_\mu = 207m_e$) have characteristic lifetimes $\tau_\mu \sim 2 \mu\text{s}$. Thus, for a magnetic field of 10 T the cyclotron frequency for muons $\omega_{c,\mu} \sim 10^9 \text{ s}^{-1}$, which means that within its lifetime a muon inside an extremely type-II superconductor can complete $\omega_{c,\mu}\tau_\mu \sim 10^3$ cyclotron orbits.

ACKNOWLEDGMENTS

This research was supported in part by a grant from the German-Israeli Foundation for Scientific Research and Development, Grant No. I-0222-136.07/91, and by the fund for the promotion of research at the Technion.

- ¹A. A. Abrikosov, Zh. Eksp. Teor. Fiz. **32**, 1442 (1957) [Sov. Phys. JETP **5**, 1174 (1957)].
- ²E. H. Brandt, J. Low Temp. Phys. **73**, 355 (1988).
- ³B. A. Dubrovin and S. P. Novikov, Sov. Math. Dokl. **22**, 240 (1980).
- ⁴A. G. Aronov, E. Altshuler, A. D. Mirlin, and P. Woelfle, Europhys. Lett. **29**, 239 (1995).
- ⁵A. A. Chernikov, M. Ya Natanzon, B. A. Petrovichev, R. Z. Sagdeev, and G. M. Zaslavski, Phys. Lett. A **122**, 39 (1987).
- ⁶G. M. Zaslavski, R. Z. Sagdeev, D. A. Usikov, and A. A. Chernikov, Sov. Phys. Usp. **31**, 887 (1988).
- ⁷M. Tabor, *Chaos and Integrability in Nonlinear Dynamics* (Wiley-Interscience, New York, 1989).
- ⁸E. J. Heller, J. Chem. Phys. **62**, 1544 (1975).
- ⁹E. J. Heller, Acc. Chem. Res. **14**, 368 (1981).
- ¹⁰E. J. Heller, in *Chaos and Quantum Physics*, edited by M. Gianconi, A. Voros, and J. Zinn Justin, Les Houches, session LII, 1989 (Elsevier, New York, 1991).
- ¹¹D. Kosloff and R. Kosloff, J. Comput. Phys. **52**, 35 (1983).
- ¹²R. Kosloff and H. Tal-Ezer, J. Chem. Phys. **81**, 3967 (1984).
- ¹³R. Kosloff, J. Phys. Chem. **92**, 2087 (1988).
- ¹⁴R. Kosloff, Annu. Rev. Phys. Chem. **45**, 145 (1994).
- ¹⁵A. Y. Rom (unpublished).
- ¹⁶D. Shonberg, *Magnetic Oscillations in Metals* (Cambridge University Press, Cambridge, England, 1984).
- ¹⁷G. Kido, K. Komorita, H. Katayama-Yoshida, and T. Takahashi, J. Phys. Chem. Solids **52**, 1465 (1991).
- ¹⁸C. M. Fowler, B. L. Freeman, W. L. Hults, J. C. King, M. Muller, and J. L. Smith, Phys. Rev. Lett. **68**, 534 (1992).
- ¹⁹F. M. Mueller, D. H. Lowndes, Y. K. Chang, A. J. Arko, and R. S. List, Phys. Rev. Lett. **68**, 3928 (1992).
- ²⁰R. Corcoran, N. Harrison, C. J. Haworth, S. M. Hayden, P. Meeson, M. Springford, and P. J. Van der Wel, Physica B **206-207**, 534 (1995).
- ²¹R. Corcoran, N. Harrison, S. M. Hayden, P. Meeson, M. Springford, and P. J. Van der Wel, Phys. Rev. Lett. **72**, 701 (1994).
- ²²E. Steep, S. Retteenberger, F. Meyer, A. G. M. Jensen, W. Joss, P. Wyder, W. Biberacher, E. Bucher, and C. S. Oglesby, Physica B **211**, 244 (1995).
- ²³D. Shonberg, J. Low Temp. Phys. **56**, 417 (1984).